Journal of Science and Technology in Civil Engineering, HUCE (NUCE), 2023, 17 (1): 79–93

EVALUATING THE PERFORMANCE OF THE RANS TURBULENCE MODELS FOR SIMULATING WAVE PROPAGATION OVER A SUBMERGED BREAKWATER USING OPENFOAM

Luong Cao Linh[a,*], Mai Cao Tri[a]

[a]*Faculty of Coastal and Offshore Engineering, Hanoi University of Civil Engineering, 55 Giai Phong road, Hai Ba Trung district, Hanoi, Vietnam*

Article history:
Received 21/02/2023, Revised 20/3/2023, Accepted 21/3/2023

Abstract

The present work is to evaluate the performance of the RANS turbulence models for simulating regular wave propagation over a submerged breakwater using the open-source Computational Fluid Dynamics (CFD) software OpenFOAM. The present numerical results of four turbulence models ($k-\varepsilon$ model, $k-\omega$ *SST* model, buoyancy-modified $k-\omega$ *SST* model, and stabilized $k-\omega$ *SST* model) are compared with published experimental data for free surface elevations and velocities at gauges. Moreover, the results of the turbulent kinetic energy (TKE) are compared and assessed between the turbulence models. Results show that the buoyancy-modified $k-\omega$ *SST* model and the stabilized $k-\omega$ *SST* model predictions agree very well with the experimental data, although the turbulence kinetic energy is still significant differences between the two models. Therefore, these two models should be used in the future for simulating the interaction between waves and submerged breakwaters.

Keywords: submerged breakwater; turbulence models; OpenFOAM/waves2foam; CFD, RANS; VOF.

https://doi.org/10.31814/stce.nuce2023-17(1)-07

1. Introduction

Submerged breakwater is an effective solution for beach protection or restoring beaches. The wave-structure interaction processes change the parameters of the wave and those are very complex. Understanding the parameters of the wave field around the submerged breakwater is essential for the design of the structure. The research method of physical models using wave flume has been applied by many authors [1–7]. The main results often are empirical formulas, the most common of which are the wave transmission coefficient formulas. The experiment's research is often not very informative about hydrodynamic characteristics and wave fields around the submerged breakwater.

In recent years, with the development of computers and software, Computational Fluid Dynamics (CFD) has become an effective tool to supplement and partially replace experimental research. Many numerical models have been developed to simulate wave-submerged structure interactions by the research of the authors such as Shen et al. [8], Peng and Zou ([9], Rahman [10], Kamath et al. [11], Liang et al. [12], Ning et al. [2], Liu et al. [4], Li and Zhang [13], Srineash et al. [14], Abdullah et al.

*Corresponding author. *E-mail address:* linhlc@huce.edu.vn (Linh, L. C.)

[15], Xu et al. [16], Kamath et al. [6]. The Reynold-Averaged Navier-Stokes (RANS) equations model can simulate well nonlinear waves and flow fields around the structure.

The turbulence models are used in the numerical models to more accurately simulate wave-submerged structure interactions, most commonly two-equation RANS turbulence models, e.g. $k-\varepsilon$ model [8], $k-\omega$ model [11], $k-\omega$ *SST* model [13]. These standard turbulence models have been demonstrated to be unconditionally unstable, and the turbulent kinetic energy (TKE) is predicted large to be excessive and might cause a significant decrease in wave height over the length of the numerical wave flume. Recently, several authors have proposed modified turbulence models to solve this problem. Devolder et al. [17, 18] proposed buoyancy-modified turbulence models that use a buoyancy term added to the TKE equation. Larsen and Fuhrman [19] proposed stabilized-modified turbulence models that use the addition of stress-limiting modification. OpenFOAM is an open-source software popular among researchers and industry, across many areas of offshore, and coastal [13, 17–19]. The library waves2foam is a plug-in toolbox to OpenFOAM [20]. Waves2foam is used to generate and absorb free surface water waves with the possibility of modeling the interaction between free surface waves and a permeable medium such as breakwaters and scour protection [19, 21–23].

Previous studies have shown that using different turbulence models will greatly affect the results in numerical models, especially for nonlinear wave problems such as breaking waves or wave-structures interaction [23, 24]. The interaction between waves and submerged breakwaters changes the parameters of the wave and those are very complex. Therefore, it is necessary to evaluate the performance of different turbulence models on wave propagation over a submerged breakwater.

In this paper, we present a study to evaluate the performance of the RANS turbulence models for simulating wave propagation over a submerged breakwater. The study uses open-source software OpenFOAM with the toolbox waves2foam [20]. The two-dimensional numerical simulation cases with four turbulence models ($k-\varepsilon$ model, $k-\omega$ *SST* model, buoyancy-modified $k-\omega$ *SST* model, and stabilized $k-\omega$ *SST* model). The paper is organized as follows. First is the introduction section. In Section 2, the governing equations for the numerical model are presented. Section 3 includes a description of the computational domain and the convergency studies of the numerical model. Subsequently, the present numerical results are compared with published experimental data and discussed in detail in Section 4. Finally, the main conclusions are drawn in Section 5.

2. Numerical method

2.1. Governing equations

The numerical model uses the incompressible RANS equations:

Mass conservation equation:

$$\frac{\partial u}{\partial x}+\frac{\partial v}{\partial y}+\frac{\partial w}{\partial z}=0 \tag{1}$$

x-component of momentum equation:

$$\begin{aligned}\frac{\partial u}{\partial t}+\frac{\partial}{\partial x}(uu)+\frac{\partial}{\partial y}(vu)+\frac{\partial}{\partial z}(wu)=&-\frac{1}{\rho}\frac{\partial p}{\partial x}+g_x+\frac{1}{\rho}\mu\left(\frac{\partial^2 u}{\partial x^2}+\frac{\partial^2 u}{\partial y^2}+\frac{\partial^2 u}{\partial z^2}\right)\\&-\left(\frac{\partial}{\partial x}\left(\overline{u'u'}\right)+\frac{\partial}{\partial y}\left(\overline{v'u'}\right)+\frac{\partial}{\partial z}\left(\overline{w'u'}\right)\right)\end{aligned} \tag{2}$$

y-component of momentum equation:

$$\frac{\partial v}{\partial t} + \frac{\partial}{\partial x}(uv) + \frac{\partial}{\partial y}(vv) + \frac{\partial}{\partial z}(wv) = -\frac{1}{\rho}\frac{\partial p}{\partial y} + g_y + \frac{1}{\rho}\mu\left(\frac{\partial^2 v}{\partial x^2} + \frac{\partial^2 v}{\partial y^2} + \frac{\partial^2 v}{\partial z^2}\right) - \left(\frac{\partial}{\partial x}\left(\overline{u'v'}\right) + \frac{\partial}{\partial y}\left(\overline{v'v'}\right) + \frac{\partial}{\partial z}\left(\overline{w'v'}\right)\right) \tag{3}$$

z-component of momentum equation:

$$\frac{\partial w}{\partial t} + \frac{\partial}{\partial x}(uw) + \frac{\partial}{\partial y}(vw) + \frac{\partial}{\partial z}(ww) = -\frac{1}{\rho}\frac{\partial p}{\partial z} + g_z + \frac{1}{\rho}\mu\left(\frac{\partial^2 w}{\partial x^2} + \frac{\partial^2 w}{\partial y^2} + \frac{\partial^2 w}{\partial z^2}\right) - \left(\frac{\partial}{\partial x}\left(\overline{u'w'}\right) + \frac{\partial}{\partial y}\left(\overline{v'w'}\right) + \frac{\partial}{\partial z}\left(\overline{w'w'}\right)\right) \tag{4}$$

where u, v, w are the Cartesian components of the fluid velocity, ρ is the fluid density, p is the pressure, g_x, g_y, g_z is the gravitational acceleration in x, y, z direction, μ is the kinematic viscosity.

The Reynolds stress tensor $\bar{\sigma}_t$ is defined as:

$$\bar{\sigma}_t = -\rho \begin{bmatrix} \overline{u'u'} & \overline{v'u'} & \overline{w'u'} \\ \overline{u'v'} & \overline{v'v'} & \overline{w'v'} \\ \overline{u'w'} & \overline{v'w'} & \overline{w'w'} \end{bmatrix} \tag{5}$$

2.2. Turbulence modeling

a. The $k-\varepsilon$ model

Turbulent kinetic energy k equation:

$$\frac{\partial k}{\partial t} + u_j\frac{\partial k}{\partial x_j} = \frac{\partial}{\partial x_j}\left[\left(\frac{\nu_t}{\sigma_k} + \nu\right)\frac{\partial k}{\partial x_j}\right] + \overline{u_i'u_j'}\frac{\partial u_i}{\partial x_j} - \varepsilon \tag{6}$$

Turbulent kinetic energy dissipation rate ε equation:

$$\frac{\partial \varepsilon}{\partial t} + u_j\frac{\partial \varepsilon}{\partial x_j} = \frac{\partial}{\partial x_j}\left[\left(\frac{\nu_t}{\sigma_\varepsilon} + \nu\right)\frac{\partial \varepsilon}{\partial x_j}\right] + C_{1\varepsilon}\frac{\varepsilon}{k}\nu_t\left(\frac{\partial u_i}{\partial x_j} + \frac{\partial u_j}{\partial x_i}\right)\frac{\partial u_i}{\partial x_j} - C_{2\varepsilon}\frac{\varepsilon}{k} \tag{7}$$

where ν_t is the turbulent kinematic viscosity, the constants for this model are: σ_k = 1.0, σ_ε = 1.3, $C_{1\varepsilon}$ = 1.44, $C_{2\varepsilon}$ = 1.92.

b. The $k-\omega$ *SST* model

In the $k-\omega$ *SST* model, the turbulence kinetic energy k and the turbulence specific dissipation rate ω are solved using two additional transport equations defined as:

$$\frac{\partial k}{\partial t} + \frac{\partial u_j k}{\partial x_j} - \frac{\partial}{\partial x_j}\left[(\nu + \sigma_k\nu_t)\frac{\partial k}{\partial x_j}\right] = P_k - \beta^*\omega k \tag{8}$$

$$\frac{\partial \omega}{\partial t} + \frac{\partial u_j \omega}{\partial x_j} - \frac{\partial}{\partial x_j}\left[(\nu + \sigma_\omega\nu_t)\frac{\partial \omega}{\partial x_j}\right] = \frac{\gamma}{\nu_t}G - \beta\omega^2 k + 2(1-F_1)\frac{\sigma_{\omega 2}}{\omega}\frac{\partial k}{\partial x_j}\frac{\partial \omega}{\partial x_j} \tag{9}$$

where P_k is the production term of k, ν_t is the turbulent kinematic viscosity.

$$\begin{aligned} P_k &= \min\left(G, 10\beta^*\omega k\right) \\ G &= \nu_t \frac{\partial u_i}{\partial x_j}\left(\frac{\partial u_i}{\partial x_j} + \frac{\partial u_j}{\partial x_i}\right) \\ \nu_t &= \frac{a_1 k}{\max\left(a_1\omega, S F_2\right)} \end{aligned} \tag{10}$$

The constants of α_k, α_ω, α and β are blended using the equation:

$$\varphi = F_1\varphi_1 + (1 - F_1)\varphi_2 \tag{11}$$

The constants for this model are: $\beta^* = 0.09$, $\alpha_1 = 5/9$, $\beta_1 = 0.075$, $\sigma_{k1} = 0.85$, $\sigma_{\omega 1} = 0.5$, $\alpha_2 = 0.44$, $\beta_2 = 0.0828$, $\sigma_{k2} = 1$, $\sigma_{\omega 2} = 0.856$.

c. The buoyancy-modified $k - \omega$ *SST* model

The buoyancy-modified $k - \omega$ *SST* model was proposed by Devolder et al. [17, 18]. The density ρ is included in two equations of the standard $k - \omega$ *SST* model and the buoyancy term G_b is added to the TKE equation.

$$\frac{\partial \rho k}{\partial t} + \frac{\partial \rho u_j k}{\partial x_j} - \frac{\partial}{\partial x_j}\left[\rho\left(\nu + \sigma_k \nu_t\right)\frac{\partial k}{\partial x_j}\right] = \rho P_k + G_b - \rho\beta^*\omega k \tag{12}$$

$$\frac{\partial \rho \omega}{\partial t} + \frac{\partial \rho u_j \omega}{\partial x_j} - \frac{\partial}{\partial x_j}\left[\rho\left(\nu + \sigma_\omega \nu_t\right)\frac{\partial \omega}{\partial x_j}\right] = \frac{\gamma}{\nu_t}\rho G - \rho\beta\omega^2 + 2\left(1 - F_1\right)\rho\frac{\sigma_{\omega 2}}{\omega}\frac{\partial k}{\partial x_j}\frac{\partial \omega}{\partial x_j} \tag{13}$$

$$G_b = -\frac{\nu_t}{\sigma_t}\frac{\partial \rho}{\partial x_j}g_j \tag{14}$$

where the buoyancy term G_b is treated implicitly, the scalar $\sigma_t = 0.85$.

d. The stabilized $k - \omega$ *SST* model

The stabilized $k - \omega$ *SST* model was proposed by Larsen and Fuhrman [19]. The buoyancy term G_b is added to the TKE equation and stress-limiting modifications to the standard $k - \omega$ *SST* model.

$$\frac{\partial \rho k}{\partial t} + \frac{\partial \rho u_j k}{\partial x_j} - \frac{\partial}{\partial x_j}\left[\rho\left(\nu + \sigma_k \nu_t\right)\frac{\partial k}{\partial x_j}\right] = \rho P_k + G_b - \rho\beta^*\omega k \tag{15}$$

$$\frac{\partial \omega}{\partial t} + \frac{\partial u_j \omega}{\partial x_j} - \frac{\partial}{\partial x_j}\left[\left(\nu + \sigma_\omega \nu_t\right)\frac{\partial \omega}{\partial x_j}\right] = \frac{\gamma}{\nu_t}G - \beta\omega^2 k + 2\left(1 - F_1\right)\frac{\sigma_{\omega 2}}{\omega}\frac{\partial k}{\partial x_j}\frac{\partial \omega}{\partial x_j} \tag{16}$$

$$\nu_t = \frac{a_1 k}{\max\left(a_1\omega, F_2\sqrt{p_0}, a_1\lambda_2\frac{\beta}{\beta^*\alpha}\frac{p_0}{p_\Omega}\omega\right)} \tag{17}$$

where λ_2 is an additional stress limiter coefficient, and the default value is 0.05.

2.3. Free surface capture

The interface between the water and the air is tracked using the volume of fluid (VOF) method [25]. The method is based on a volume fraction coefficient α, which is 0 for air and 1 for water. The volume fraction is solved by an advection equation:

$$\frac{\partial \alpha}{\partial t} + \frac{\partial\left(\alpha u_i\right)}{\partial x_i} + \frac{\partial\left[\alpha\left(1 - \alpha\right)u_{ir}\right]}{\partial x_i} = 0 \tag{18}$$

where u_{ir} is the relative velocity between the water phase and the air phase.

The density and kinematic viscosity at the interface is obtained by a weighted value based on the volume fraction coefficient.

$$\begin{aligned} \rho &= \alpha\rho_w + (1-\alpha)\rho_a \\ \nu &= \alpha\nu_w + (1-\alpha)\nu_a \end{aligned} \tag{19}$$

where ρ_w and ρ_a are the densities of water and air, $\nu_w$and ν_a are the kinematic viscosity coefficients of water and air.

2.4. Relaxation method

The wave relaxation zone technique was presented by Jacobsen et al. [20] in the waves2foam toolbox. Relaxation zones are implemented to avoid wave reflection at the inlet and outlet boundaries. The relaxation function is in the following way:

$$\varphi = \gamma_R\varphi_{computed} + (1-\gamma_R)\varphi_{\text{target}} \tag{20}$$

where φ is either velocity u_i or volume fraction α, γ_R is the weighting factor defined as:

$$\gamma_R(\chi_R) = 1 - \frac{\exp\left(\chi_R^{3.5}\right) - 1}{\exp(1) - 1} \quad for \quad \chi_R \in [0,\ 1] \tag{21}$$

3. Numerical implementation

3.1. Computational domain

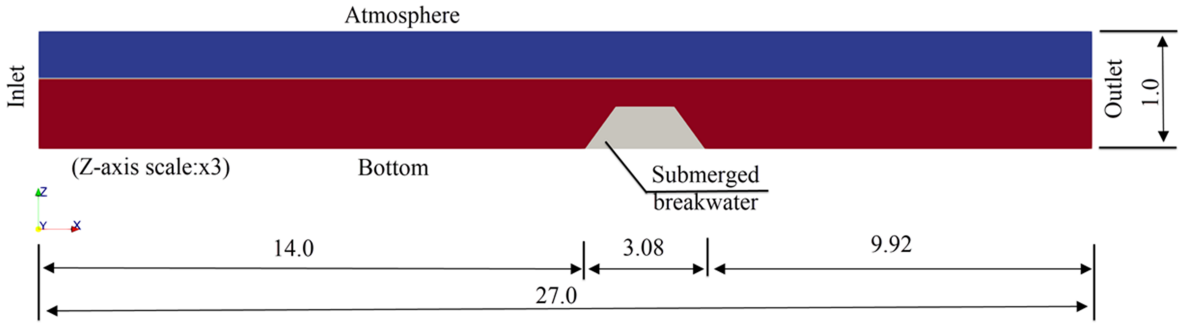

Figure 1. The dimensions of the numerical wave tank, units (m)

The numerical model setup is accorded to the setup from the physical experiment conducted by Liu et al. [4]. The dimensions of the numerical wave tank (NWT) are shown in Fig. 1. The length of NWT is reduced compared to those of the physical wave flume to decrease the computational domain. The water depth of the NWT is 0.6 m. A regular wave test case is selected from experimental data with a wave height of 0.1 m and a wave period of 2.2 s, and 2^{nd} order Stokes theory is used for all the simulation cases presented. A relaxation zone of approximately one wavelength, L, is applied at the inlet and outlet boundary. Six wave gauges (W1-6) and three velocity gauges (V1-3) are placed at the same locations as the experimental, as shown in Fig. 2.

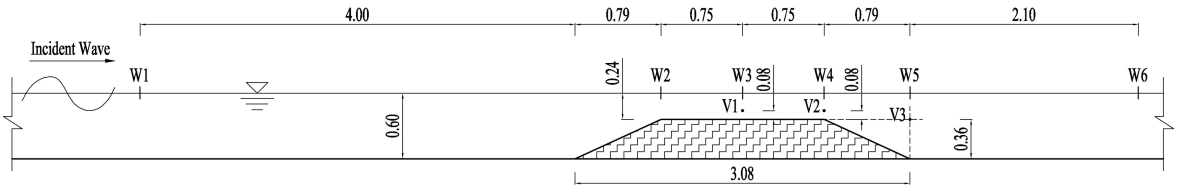

Figure 2. Locations of gauges, units (m)

3.2. *Boundary conditions*

The types of boundary conditions for this simulation are given in Fig. 1: inlet on the left, outlet on the right, and atmosphere on the top. The bottom and the structure's surface are modeled as smooth solid walls. The no-slip condition for velocity and zero gradient condition for pressure is employed in the front, back, bottom, and structure's surface boundaries. The velocity is specified based on the 2nd order Stokes wave theory at the inlet boundary. At the outlet boundary, both the water and air velocities are set to zero. At the atmosphere boundary, the *pressureInletOutletVelocity* is applied to the velocity.

3.3. *Convergence study*

This study performs spatial and temporal convergence studies for the numerical wave tank without structure. All the present simulations are performed for 50 seconds. The free surface elevations at the six probes are used as metrics in the convergence studies.

For the spatial convergence study, the grid size in the free surface region is refined, as shown in Fig. 3. The vertical cell size is normalized by the wave height, and the horizontal cell size ensures an aspect ratio of 1. In this study, three size options are chosen: 5, 10, and 20 cells per wave height (CPH) [26].

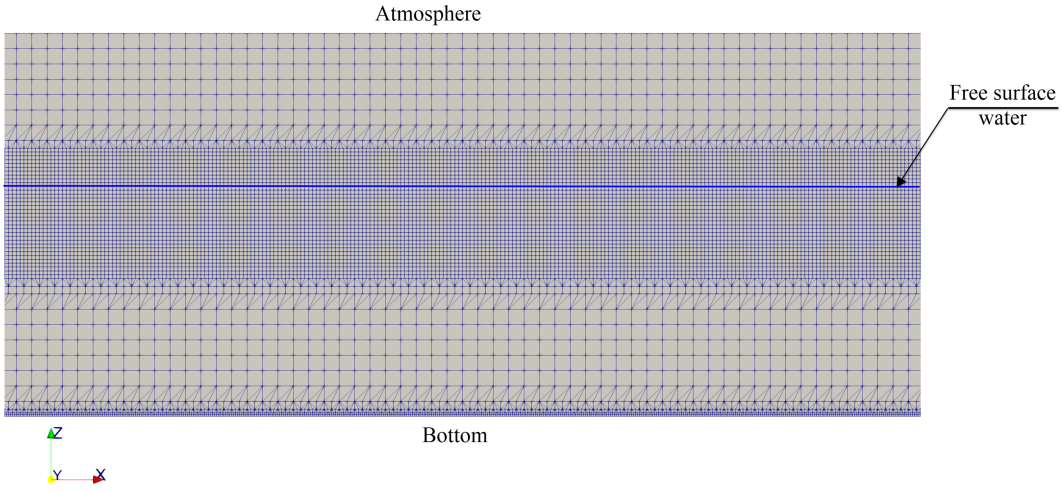

Figure 3. The mesh around the free surface

For the temporal convergence study, the time step is varied by controlling the maximum Courant number ($Co_{\max}$). In this study, three $Co_{\max}$ are used: 0.25, 0.50, and 1.00. Thus, different meshes and $Co_{\max}$ cases are shown in Table 1.

Table 1. Parameters of convergence study cases

Cases	Mesh 1	Mesh 2	Mesh 3
Minimum vertical cell size Δz (m)	0.020	0.010	0.005
CPH	5	10	20
Number of Cells	97852	190350	519075
Co_{max}	0.5	0.25/0.5/1.0	0.5

Simulation results corresponding to three mesh sizes with $Co_{\max}$ of 0.5 are shown in Fig. 4. Free surface elevations at six gauges (W1-W6) are shown as full-time simulations and magnified views. The results show good agreement with comparing three mesh sizes, only differences can be observed in the magnified view versions. The relative errors of peak free surface elevations (averaged over the last ten wave periods of simulation) are shown in Fig. 6(a), where, ε_{12} is the relative error between Mesh 1 and Mesh 2, ε_{23} is the relative error between Mesh 2 and Mesh 3. The results show that the mesh size option of 10CPH is sufficient for accuracy for spatial convergence.

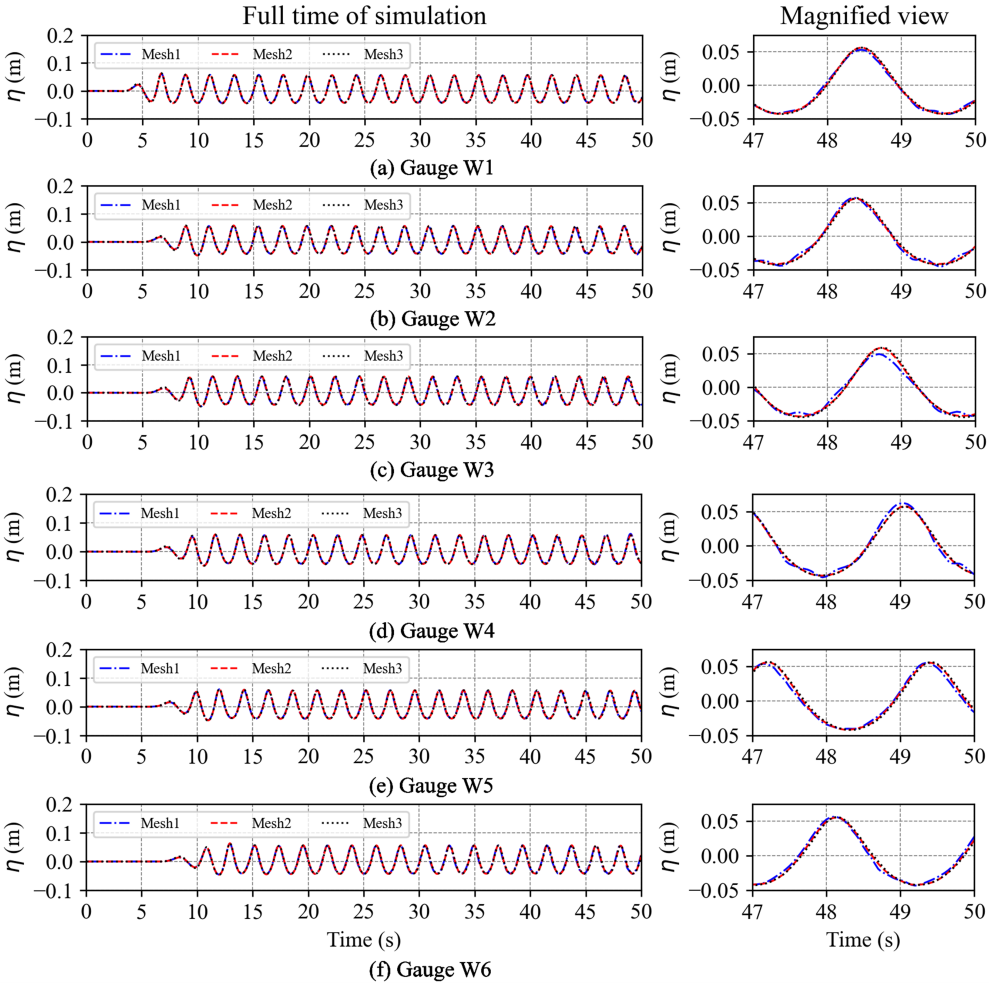

Figure 4. Free surface elevations at wave gauges with three mesh cases

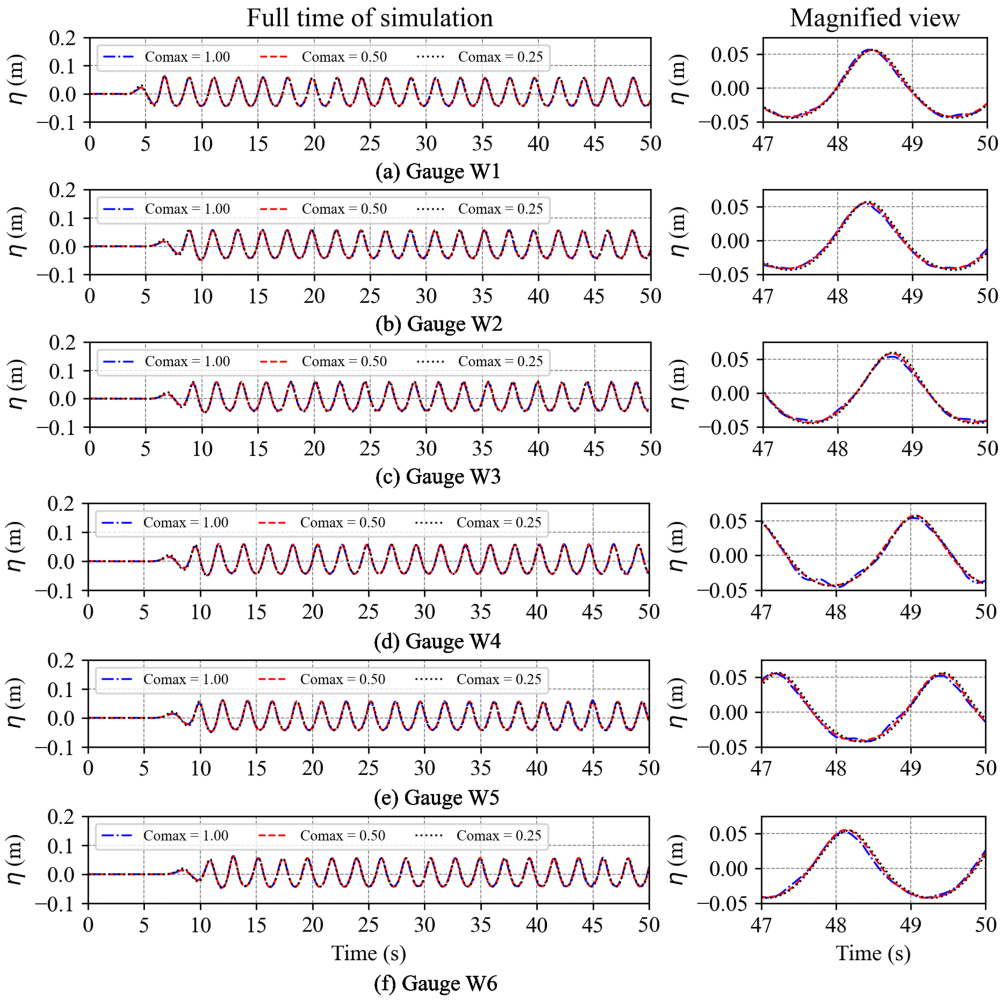

Figure 5. Free surface elevations at wave gauges with three Courant number

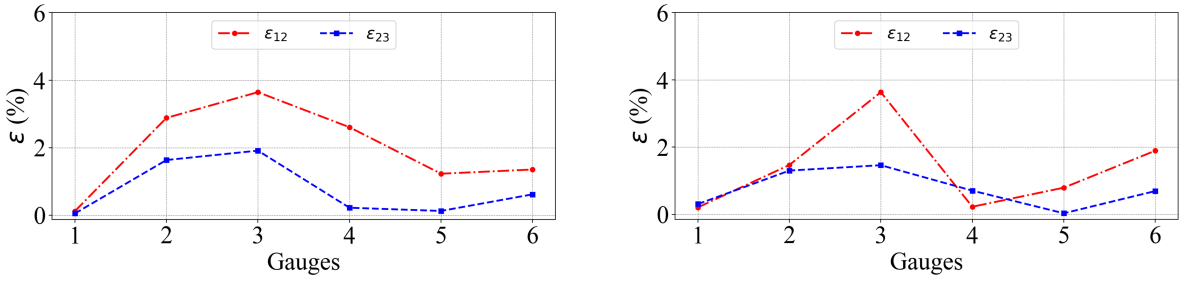

(a) Spatial convergence study

(b) Temporal convergence study

Figure 6. The relative error between the results of the convergence study cases

Similarly, the results corresponding to three $Co_{\max}$ cases with Mesh 2 option are shown in Fig. 5. The relative errors of peak free surface elevations are shown in Fig. 6(b), where, ε_{12} is the relative error between $Co_{\max}$ = 1.0 and $Co_{\max}$ = 0.5, ε_{23} is the relative error between $Co_{\max}$ = 0.5 and $Co_{\max}$

= 0.25. The results show only small differences with $Co_{\max}$ = 1.0 case, and good agreement between the other two maximum Courant number cases. Thus, $Co_{\max}$ = 0.5 case is sufficient for accuracy for temporal convergence.

Therefore, the mesh size option of 10CPH and an aspect ratio of 1 (in the free surface region) with a maximum Courant number of 0.5 is chosen and will be used in subsequent simulations.

4. Results and discussion

In this study, four simulations corresponding to four turbulence models are conducted. The numerical results of free surface elevations and velocities at gauges are compared with experimental data from Liu et al. [4]. Moreover, the results of the turbulent kinetic energy (TKE) are compared and assessed between the turbulence models. All the present simulations are performed for 50 seconds. The simulation time is chosen to ensure that the waves in the NWT fully develop and become stable, and the results after that point have a sufficiently long time interval corresponding to the experimental data, for free surface elevations of 10 seconds and the horizontal velocity of 5 wave periods.

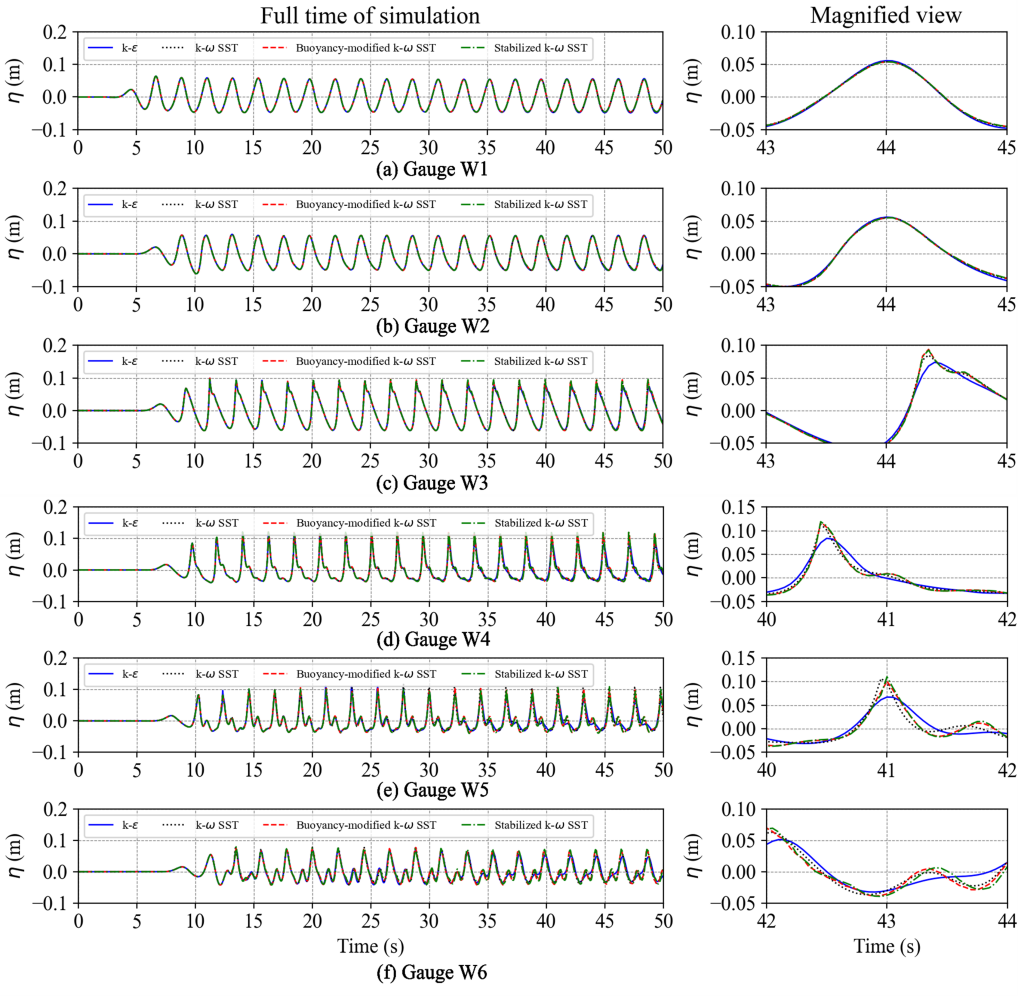

Figure 7. Free surface elevations at wave gauges with four turbulence models

The root means square error (RMSE) for free surface elevations and horizontal velocities is used to compare the performance of the various turbulence models.

$$RMSE = \sqrt{\frac{\sum_{i=1}^{n}\left(X_{num} - X_{exp}\right)^2}{n}} \tag{22}$$

where n is the number of data, X_{num} is the numerical model results, and X_{exp} is the experimental value.

4.1. Free surface elevation

Fig. 7 presents the comparison of free surface elevations at six wave gauges (W1-W6) between four numerical simulations corresponding to four turbulence models. The results are shown as full-time simulations and magnified views.

It is seen that good agreement between all numerical models at the two first probe locations (Fig. 7(a) and (b)), at the remaining four probe locations, shows the significant discrepancy between the $k-\varepsilon$ model and the other three turbulence models (Fig. 7(c), (d), (e) and (f)).

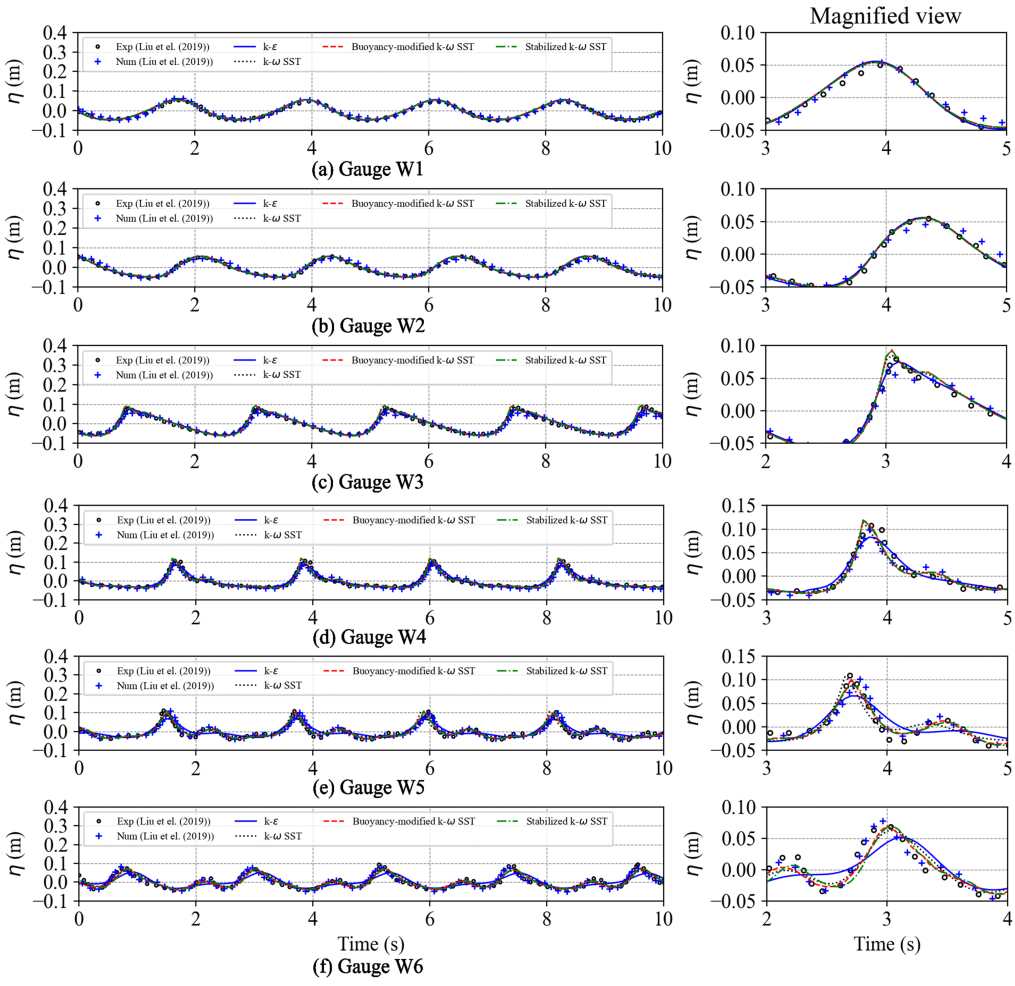

Figure 8. Comparison of free surface elevation between numerical models and experimental data

Fig. 8 shows the numerical results and the corresponding experimental data in ten seconds at six wave gauges. Note, for experimental data, $t = 0$ s is defined as after the wave has fully developed and becomes stable, for present numerical models, results obtained in ten seconds near the end of the simulation time are used for comparison.

Prediction of all the numerical models shows good agreement in the free surface compared to experimental data at two wave probes in front of the submerged breakwater. However, the $k-\varepsilon$ model predicted was poorly accurate at four other wave probes, especially the last two (Fig. 8(e) and (f)). Three other turbulent models generally show reasonably well with experimental data. The $k-\omega$ *SST* model predicted a significantly different secondary wave at the fifth wave gauge (W5).

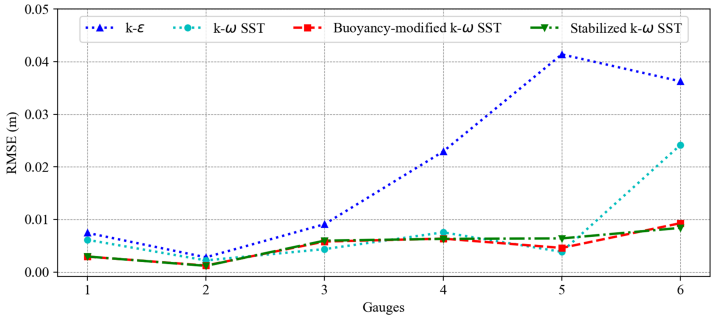

Figure 9. RMSE of peak free surface elevations with four turbulence models

Fig. 9 shows RMSE results of peak free surface elevations at six gauges. The buoyancy-modified $k-\omega$ *SST* and the stabilized $k-\omega$ *SST* models are almost the same at all wave gauges and agree best with the experimental data.

4.2. Velocity

Fig. 10 and Fig. 11 compare horizontal and vertical velocities at three gauges (V1-V3) between four turbulence models. The results are shown as full-time simulations and magnified views. The results show that, similar to the free surface elevation, the $k-\varepsilon$ model has a significant discrepancy compared to the three other turbulence models.

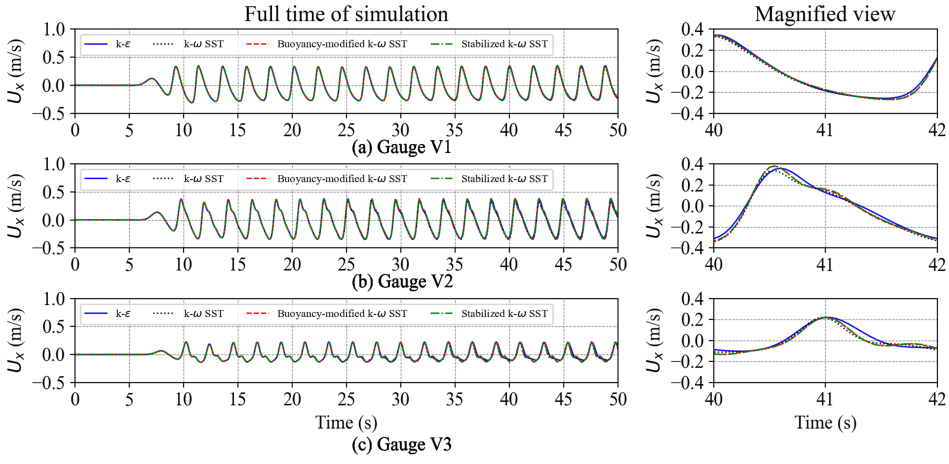

Figure 10. Time series of horizontal velocities with four turbulence models

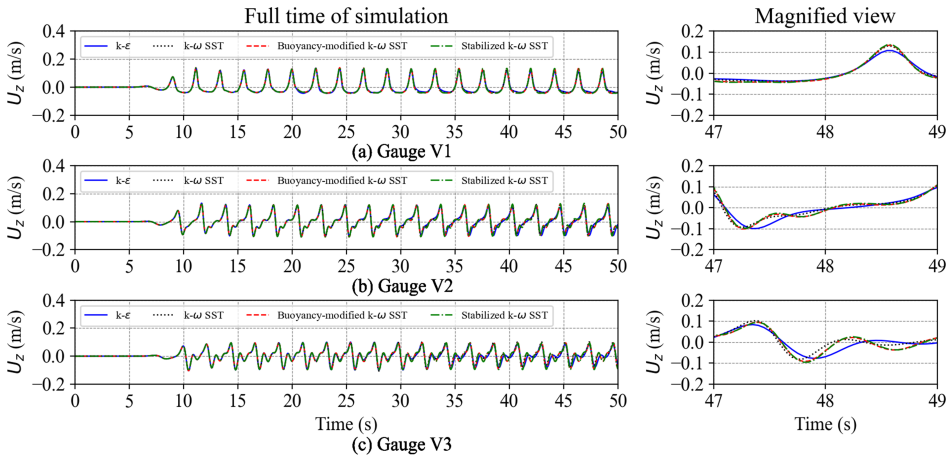

Figure 11. Time series of vertical velocities with four turbulence models

Fig. 12 presents the comparison of horizontal velocities between numerical models and experimental data in five wave periods, where t/T is the normalized time.

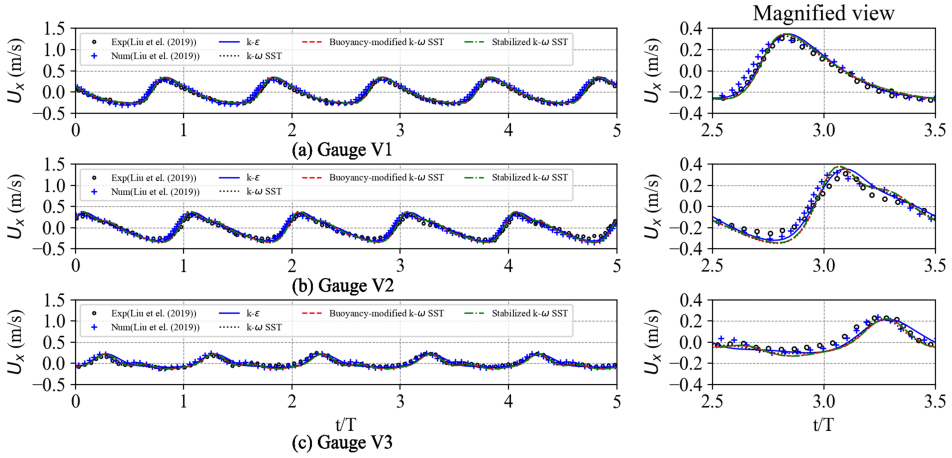

Figure 12. Comparison of horizontal velocities between numerical models and experimental data

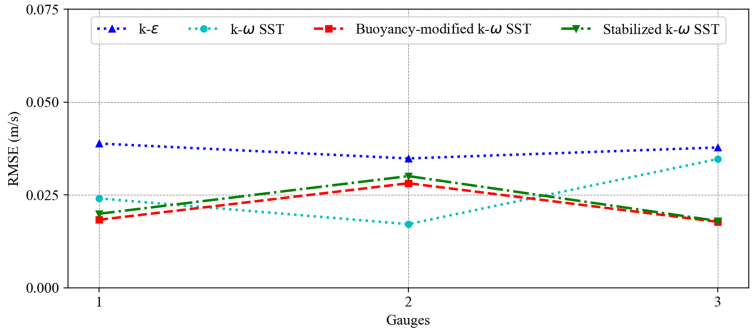

Figure 13. RMSE of peak horizontal velocities with four turbulence models

Fig. 13 shows RMSE results of peak horizontal velocities at three gauges. It is seen that the three turbulence models ($k-\omega$ *SST*, buoyancy-modified $k-\omega$ *SST* and stabilized $k-\omega$ *SST*) agree well with the experimental data at all probes.

4.3. Turbulent behavior

The turbulent behavior of turbulence models is judged through TKE k analysis. Fig. 14 shows the contour plot of the TKE of the four turbulence models. It is seen that the $k-\varepsilon$ model predicted the TKE largest, followed by the $k-\omega$ *SST* model and buoyancy-modified $k-\omega$ *SST*, and the stabilized $k-\omega$ *SST* model predicted the TKE smallest.

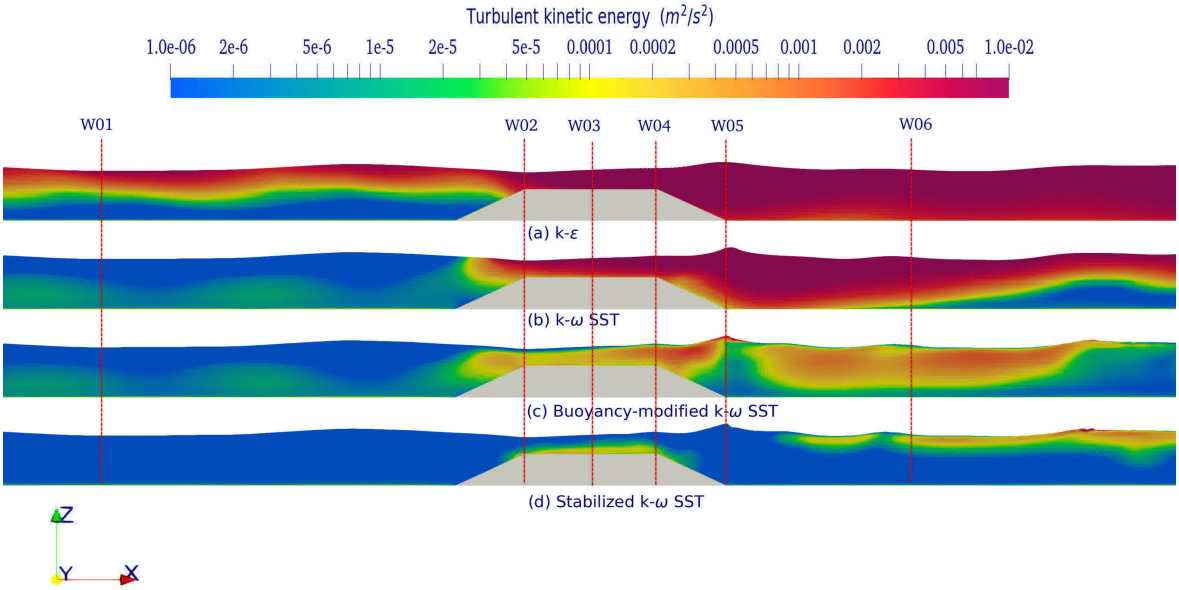

Figure 14. Snapshots of the turbulent kinetic energy k (m^2/s^2) with four turbulence models

As can be seen, the $k-\omega$ *SST* model and the buoyancy-modified $k-\omega$ *SST* model give almost the same results in the wave propagating zone in front of the structure. For the $k-\omega$ *SST* model, the TKE is pretty large in the above and behind the dike, which does not affect the prediction results of the prime wave much but significantly affects the prediction results of the secondary wave. This is improved when using the buoyancy-modified $k-\omega$ *SST* or the stabilized $k-\omega$ *SST* model. There is a significant difference in TKE prediction between the buoyancy-modified $k-\omega$ *SST* model and the stabilized $k-\omega$ *SST* model, but it does not affect the results of free surface elevations and the velocity results at gauges, the results are almost the same between the two turbulence models.

Numerical models give results consistent with previous studies. The standard turbulent models ($k-\varepsilon$, $k-\omega$ *SST*) are demonstrated which results in the exponential growth of the TKE and eddy viscosity [19]. The modified turbulent models (buoyancy-modified $k-\omega$ *SST*, stabilized $k-\omega$ *SST*) significantly reduce the TKE [17–19].

The turbulent kinetic energy is a component of total kinetic energy that will be diffused and dissipated by viscous forces during wave propagation. Therefore, the larger the turbulent kinetic energy, the faster the total kinetic energy decreases, leading to the corresponding decrease in potential energy. As a result, the free surface elevations also decrease [23]. For the $k-\varepsilon$ model, the TKE phenomenon

large to excessive is the cause of wave height decline as discussed in free surface elevations. Consequently, there was no wave breaking as observed in the three other numerical models.

5. Conclusions

In this paper, we analyzed four RANS turbulence models that predicted waves through submerged breakwater using open-source CFD software OpenFOAM with the toolbox waves2foam. In the present study, the results of numerical models are compared to published experimental data, from this, the main conclusions are drawn as follows:

(i) The $k-\varepsilon$ model over-predicts turbulent kinetic energy leading to wave height attenuation during wave propagation through the submerged breakwater.

(ii) The $k-\omega$ *SST* model predicts free surface elevations and velocities pretty well, although the turbulent kinetic energy is still quite large, especially at the fluid field behind the dike, the significant error is the result of the prediction of the secondary wave.

(iii) The buoyancy-modified $k-\omega$ *SST* model and the stabilized $k-\omega$ *SST* model predict free surface elevations and velocities almost the same and agree well with the experimental data, although the turbulence kinetic energy is still significant differences between the two models.

Thus, open-source CFD software OpenFOAM/waves2foam with turbulent models, i.e. the buoyancy-modified $k-\omega$ *SST* and stabilized $k-\omega$ *SST* models, can be applied to simulate the interaction of waves and submerged breakwaters.

Acknowledgments

The author sincerely thanks the financial support of the Hanoi University of Civil Engineering for the research "Study on the wave reduction efficiency of submerged breakwater using numerical method", number 31-2022/KHXD.

References

[1] Lokesha, Kerpen, N. B., Sannasiraj, S. A., Sundar, V., Schlurmann, T. (2015). Experimental Investigations on Wave Transmission at Submerged Breakwater with Smooth and Stepped Slopes. *Procedia Engineering*, 116:713–719.

[2] Ning, D., Chen, L., Zhao, M., Teng, B. (2016). Experimental and Numerical Investigation of the Hydrodynamic Characteristics of Submerged Breakwaters in Waves. *Journal of Coastal Research*, 320: 800–813.

[3] Kubowicz-Grajewska, A. (2016). Experimental investigation into wave interaction with a rubble-mound submerged breakwater (case study). *Journal of Marine Science and Technology*, 22(2):313–326.

[4] jin Liu, B., Cheng, D., chen Sun, Z., zeng Zhao, X., Chen, Y., dong Lin, W. (2019). Experimental and numerical study of regular waves past a submerged breakwater. *Journal of Hydrodynamics*, 31(4):641–653.

[5] Jafarzadeh, E., Kabiri-Samani, A., Mansourzadeh, S., Bohluly, A. (2020). Experimental modeling of the interaction between waves and submerged flexible mound breakwaters. *Proceedings of the Institution of Mechanical Engineers, Part M: Journal of Engineering for the Maritime Environment*, 235(1):127–141.

[6] Kamath, A., Roy, T., Seiffert, B. R., Bihs, H. (2022). Experimental and Numerical Study of Waves Breaking Over a Submerged Three-Dimensional Bar. *Journal of Waterway, Port, Coastal, and Ocean Engineering*, 148(2).

[7] Tuan, V. M., Duong, B., Hung, V. Q., Manh, N. D., Linh, N. M. (2022). Experimental study on the wave dissipation performance of a perforated semi-circular floating breakwater. *Journal of Science and Technology in Civil Engineering (STCE) - HUCE*, 16(3):59–70.

[8] Shen, Y. M., Ng, C. O., Zheng, Y. H. (2004). Simulation of wave propagation over a submerged bar using the VOF method with a two-equation k–ϵ turbulence modeling. *Ocean Engineering*, 31(1):87–95.

[9] Peng, Z., Zou, Q. (2008). Numerical analysis of wave transformation over low-crested impermeable breakwater. In *The Eighteenth International Offshore and Polar Engineering Conference*, OnePetro, 672–677.

[10] Rahman, M. A. (2013). Experimental and Numerical Investigation on Wave Interaction with Submerged Breakwater. *Journal of Water Resources and Ocean Science*, 2(6):155.

[11] Kamath, A., Bihs, H., Chella, M. A., Arntsen, Ø. A. (2015). CFD Simulations of Wave Propagation and Shoaling over a Submerged Bar. *Aquatic Procedia*, 4:308–316.

[12] Liang, B., Wu, G., Liu, F., Fan, H., Li, H. (2015). Numerical study of wave transmission over double submerged breakwaters using non-hydrostatic wave model. *Oceanologia*, 57(4):308–317.

[13] Li, X., Zhang, W. (2019). 3D numerical simulation of wave transmission for low-crested and submerged breakwaters. *Coastal Engineering*, 152:103517.

[14] Srineash, V. K., Kamath, A., Murali, K., Bihs, H. (2020). Numerical Simulation of Wave Interaction with Submerged Porous Structures and Application for Coastal Resilience. *Journal of Coastal Research*, 36 (4):752.

[15] Abdullah, S. F., Fitriadhy, A., Desa, S. M. (2021). Numerical and experimental investigations of wave transmission behind a submerged WABCORE breakwater in low wave regime. *Journal of Ocean Engineering and Marine Energy*, 7(4):405–420.

[16] Xu, T.-J., Wang, X.-R., Guo, W.-J., Dong, G.-H., Hou, H.-M. (2020). Numerical simulation of combined effect of pneumatic breakwater and submerged breakwater on wave damping. *Ships and Offshore Structures*, 17(2):242–256.

[17] Devolder, B., Rauwoens, P., Troch, P. (2017). Application of a buoyancy-modified k-ω SST turbulence model to simulate wave run-up around a monopile subjected to regular waves using OpenFOAM ®. *Coastal Engineering*, 125:81–94.

[18] Devolder, B., Troch, P., Rauwoens, P. (2018). Performance of a buoyancy-modified k-ω and k-ω SST turbulence model for simulating wave breaking under regular waves using OpenFOAM®. *Coastal Engineering*, 138:49–65.

[19] Larsen, B. E., Fuhrman, D. R. (2018). On the over-production of turbulence beneath surface waves in Reynolds-averaged Navier–Stokes models. *Journal of Fluid Mechanics*, 853:419–460.

[20] Jacobsen, N. G., Fuhrman, D. R., Fredsøe, J. (2011). A wave generation toolbox for the open-source CFD library: OpenFoam®. *International Journal for Numerical Methods in Fluids*, 70(9):1073–1088.

[21] Kazakis, I., Karambas, T. V. (2023). Numerical Simulation of Hydrodynamics and Sediment Transport in the Surf and Swash Zone Using OpenFOAM®. *Journal of Marine Science and Engineering*, 11(2):446.

[22] Jin, H., Liu, Y., He, S.-y., Li, H.-j. (2014). Numerical study on the wave dissipating performance of a submerged horizontal plate breakwater using OpenFOAM. In *The Eleventh ISOPE Pacific/Asia Offshore Mechanics Symposium*, OnePetro.

[23] Qu, S., Liu, S., Ong, M. C. (2021). An evaluation of different RANS turbulence models for simulating breaking waves past a vertical cylinder. *Ocean Engineering*, 234:109195.

[24] Brown, S. A., Greaves, D. M., Magar, V., Conley, D. C. (2016). Evaluation of turbulence closure models under spilling and plunging breakers in the surf zone. *Coastal Engineering*, 114:177–193.

[25] Hirt, C. W., Nichols, B. D. (1981). Volume of fluid (VOF) method for the dynamics of free boundaries. *Journal of Computational Physics*, 39(1):201–225.

[26] Schmitt, P., Windt, C., Davidson, J., Ringwood, J. V., Whittaker, T. (2020). Beyond VoF: alternative OpenFOAM solvers for numerical wave tanks. *Journal of Ocean Engineering and Marine Energy*, 6(3): 277–292.